Experimental Charge Density Analysis and Electrostatic Properties of Crystalline 1,3-Bis(Dimethylamino)Squaraine and Its Dihydrate from Low Temperature (T = 18 and 20 K) XRD Data

Riccardo Destro [1,*], **Pietro Roversi** [2], **Raffaella Soave** [3], **Arjan Hovestad** [4] **and Leonardo Lo Presti** [1]

1   Department of Chemistry, Università degli Studi di Milano, Via Golgi 19, 20133 Milano, Italy;
    leonardo.lopresti@unimi.it
2   Leicester Institute of Structural and Chemical Biology, Department of Molecular and Cell Biology, University
    of Leicester, Lancaster Road, Leicester LE1 7HB, UK; pr159@leicester.ac.uk
3   Istituto di Scienze e Tecnologie Chimiche "Giulio Natta" (SCITEC), Italian Research Council, Via Golgi 19,
    20133 Milano, Italy; raffaella.soave@scitec.cnr.it
4   MECO Equipment Engineers B.V., Marconilaan 2, 5151 DR Drunen, The Netherlands;
    arjan.hovestad@besi.com
*   Correspondence: riccardo.destro@unimi.it

check for updates

Abstract: Multipolar refinements of structural models fitting extensive sets of X-ray diffraction (XRD) data from single crystals of 1,3-bis(dimethylamino)squaraine [SQ, $C_8H_{12}N_2O_2$] and its dihydrate [SQDH, $C_8H_{12}N_2O_2 \cdot 2H_2O$], collected at very low T (18 ± 1 K for SQ, 20 ± 1 K for SQDH), led to an accurate description of their crystal electron density distributions. Atomic volumes and charges have been estimated from the experimental charge densities using the Quantum Theory of Atoms in Molecules (QTAIM) formalism. Our analysis confirms the common representation (in the literature and textbooks) of the squaraine central, four-membered squarylium ring as carrying two positive charges, a representation that has been recently questioned by some theoretical calculations: the integrated total charge on the C4 fragment is estimated as ca. +2.4e in SQ and +2.2e in SQDH. The topology of the experimental electron density for the SQ squaraine molecule is modified in the dihydrated crystal by interactions between the methyl groups and the H_2O molecules in the crystal. Maps of the molecular electrostatic potential in the main molecular planes in both crystals clearly reveal the quadrupolar charge distribution of the squaraine molecules. Molecular quadrupole tensors, as calculated with the PAMoC package using both Stewart and QTAIM distributed multipole analysis (DMA), are the same within experimental error.

Keywords: single crystal; X-ray diffraction; charge density; squaraine; low temperature; Quantum Theory of Atoms in Molecules; non–covalent interactions; electrostatics

1. Introduction

In his extensive review on the reactivity of squaric acid, Schmidt named "squaraines" the 1,3-disubstituted squaric acid derivatives containing delocalized bonds. The same year (1980), this author published another ample review, specifically devoted to the chemistry of squaraines [1,2], a topic that has since been subjected to many studies, owing to the large variety of squaraine-derived materials that are useful for many applications. Indeed, last year (2019) as many as three distinct reviews on squaraines have appeared in the literature [3], not to mention publications describing

numerous individual experimental and/or theoretical studies [4–6]. Yet, "while the technological uses of squaraines are extensive and a large number of squaraines have been synthesized and found to be useful, very little is known about the fundamental properties of squaraines,". This statement was made many years ago [7], but it appears to be still valid: a simple search of the SciFinder database [8], finds no references containing both the "fundamental properties" and "squaraines" keywords, out of 2303 positive hits for the "squaraines" keyword alone.

In the present paper, we report the results of our investigation of the electrostatic properties of 1,3-bis(dimethylamino)-squaraine (hereinafter SQ) and its dihydrate (SQDH), as obtained by X-ray diffraction (XRD) experimental charge density analysis. The asymmetric unit of SQ is made up of half of a squaraine molecule (for a total of twelve atoms), the centre of inversion of the molecule sitting on the inversion centre at the $\bar{1}$ site of space group Pbcn. The asymmetric unit of SQDH includes two half molecules of squaraine, each centred on a distinct centre of symmetry of space group $P2_1/c$, plus two water molecules, hence thirty atoms in all.

The crystals of both compounds were studied in our laboratory several years ago at room temperature, first obtaining the geometry and the molecular parameters of SQ [9,10], then establishing the structure and the stability of SQ and its di- and tetra-hydrates [11], by using XRD, IR spectroscopy and thermodynamic measurements. Here, our study is based on extensive sets of low-T XRD data (T = 18 ± 1 K for SQ and T = 20 ± 1 K for SQDH), and concerns the main features of the crystalline electron density distribution, the corresponding electrostatic potential, the quadrupole moments of the squaraine molecules, and the dipole and quadrupole moments of the water molecules in the crystal. It is well documented that the role of electrostatics is essential to interpret the structural features of squaraine aggregates, as well as to understand unusual properties of centrosymmetric squaraines and the features of materials including squaraine frameworks [12–14], particularly the so-called quadrupolar dyes. Experimental as well as theoretical and computational work on these materials is published regularly [15–19].

Our first report [9] on SQ (where the squaraine was labeled DMASQ) included the study of its isomer 3,4-bis(dimethylamino)-3-cyclobutene-1,2-dione (DMACB). Common features of both crystal structures are columns of stacked molecules extending along the shortest axis of the crystal, and numerous CH···O interactions. Owing to the similarities between SQ and DMACB, and since it was known that DMACB crystals undergo a reversible phase transition at T = 147 K [20], a preliminary step of the present investigation has been the determination of the cell dimensions of the SQ crystals at several temperatures from 293 down to 18 K. No anomalies were detected and the occurrence of a phase transition was excluded.

As described in the next "Experimental" section, using a SQ crystal at 18 K we measured extensive sets of diffracted intensities, then analysed with the VALRAY set of programs. The same procedure was adopted for the study of SQDH (named SQ2 in [11]) [21], for which the temperature of data measurements was 20 K. After multipole refinements of the corrected intensities, the electrostatic properties of the two crystals were evaluated and compared, as reported in the following section "Results and Discussion". A brief "Conclusions" section ends our report.

2. Materials and Methods

The procedures for the synthesis and the crystallization of SQ and SQDH have been reported in our previous papers. The crystals of SQ are highly hygroscopic [9,11]: if left in contact with atmospheric moisture during or after crystallization they become whitish and show, on Weissenberg films, lines typical of powder diffractograms, in addition to the regular diffraction pattern of a single crystal. The powder lines were found to be due to the dihydrate SQDH.

2.1. Cell Dimensions

Samples of SQ and SQDH accurately sealed into capillaries remained intact and transparent, without giving rise to powder lines on films, for several weeks. One of the samples of SQ was used

to determine the cell dimensions at six different temperatures, from RT down to 18 K, at which temperature the X-ray data collection took place. The temperature dependence of the cell parameters is reported in Table 1 and in Figure 1. Details of the instrumental settings and of the measurement procedure were the same as those reported for the study of the solid-solid phase transition (at 147 K) of DMACB, that is the isomer of SQ [20]. The smooth dependence of the cell parameters with T, with no discontinuities nor sudden changes of slope, together with the absence of superlattice reflections, and the fact that the space group of each crystal form is the same at RT and 18 K, makes the occurrence of phase transitions in the investigated temperature range very unlikely. The dimensions of the SQDH cell at five different temperatures in the range 20–298 K, and their T dependence, are also reported in Table 1 and Figure 1.

Table 1. Cell dimensions [a] of SQ and SQDH.

T/K [b]	a/Å	b/Å	c/Å	β/°	V/Å3
			SQ		
293	15.217(3)	8.162(2)	6.986(1)	90. [c]	867.8(3)
230	15.177(4)	8.102(2)	6.945(2)	90. [c]	854.0(4)
174	15.139(4)	8.059(2)	6.909(2)	90. [c]	843.0(4)
117	15.106(3)	8.023(1)	6.879(1)	90. [c]	833.8(3)
67.5	15.081(5)	8.002(3)	6.857(3)	90. [c]	827.5(5)
18	15.072(2)	7.9873(9)	6.8410(9)	90. [c]	823.5(2)
			SQDH		
298	8.031(1)	7.492(5)	17.809(6)	90.98(1)	1071.3(7)
293	8.025(1)	7.485(1)	17.797(3)	90.98(2)	1068.9(3)
79	7.959(3)	7.198(3)	17.797(6)	91.59(1)	1019.2(7)
25.5	7.955(5)	7.155(4)	17.802(4)	91.65(1)	1012.8(9)
20	7.959(1)	7.154(1)	17.799(2)	91.69(1)	1013.0(2)

[a] Estimated standard deviations (esd's) in the last significant digit are in parentheses. [b] Maximum uncertainty = 1 K. [c] Orthorhombic structure: β is constrained to 90° by symmetry.
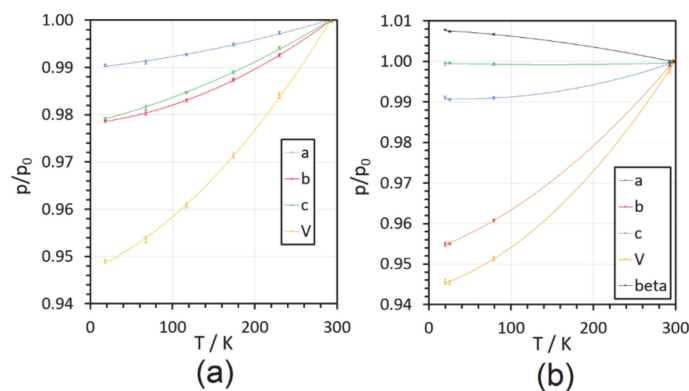

Figure 1. (**a**) Relative changes of lattice parameters (p = a, b, c, V) of SQ in the T range 18–293 K with respect to room temperature (p_0). Vertical bars correspond to 1 estimated standard deviation (esd) and full lines come from linear least squares fittings with 2nd order polynomials (average R = 0.999). (**b**) Same as (**a**), for SQDH in the range 20–293 K. Average R = 0.999 with the exclusion of c, which does not appreciably change with T.

2.2. Data Collection

Diffracted intensities of the two compounds were measured, by ω-2θ scans, on two different four-circle diffractometers equipped with our local version of the Samson cryostat and conventional point detectors [22,23]. The data collection strategy adopted in the case of glycine was also applied for the SQ crystal [24]: measurements of the intensity data for the hemisphere h ≥ 0 (here out to 2θ = 109

deg) followed by re-measurement of low-angle data at a lower current setting, to minimize possible problems associated with nonlinearity of the photon counting system.

A similar low-angle collection was performed in the case of the di-hydrate crystal, for which a full hemisphere was scanned up to $2\theta = 90$ deg, plus one quadrant for $90 \le 2\theta \le 109$ deg; in the $2\theta > 60$ deg range, only reflections with intensities above a threshold limit (1000 counts of raw integrated intensity) were kept as measured data.

No significant decay of either sample was detected. Likely, the extremely low temperatures (18–20 K) at which the experiments were performed helped to avoid serious radiation damage. All intensity measurements were corrected for scan-truncation losses according to an empirical method based on profile analyses and background distributions as a function of 2θ[23,25,26]. Corrections were made for Lorentz and polarization effects, but not for absorption, which was presumably negligible ($\mu = 0.0895$ mm^{-1} for SQ and $\mu = 0.101$ mm^{-1} for SQDH). The data collection and processing statistics for the two crystals are reported in Table 2. CCDC 2020258 and CCDC 2020259 entries contain the supplementary crystallographic data, respectively, for SQ and SQDH. The data can be obtained free of charge from The Cambridge Crystallographic Data Centre via www.ccdc.cam.ac.uk/structures (also see Supplementary Materials).

Table 2. Low-T crystal data of 1,3-bis(dimethylamino)squaraine (SQ) and its di-hydrate (SQDH).

Compound	SQ	SQDH
Sample Information		
Empirical formula	$C_8H_{12}N_2O_2$	$C_8H_{12}N_2O_2{\cdot}2H_2O$
Formula wt/g mol^{-1}	168.22	204.23
Crystal system	Orthorhombic	Monoclinic
Space group	Pbcn	P2$_1$/c
Z	4	4
T/K	18 (1)	20 (1)
a/Å	15.072 (2)	7.959 (2)
b/Å	7.9873 (9)	7.154 (1)
c/Å	6.8410 (9)	17.799 (2)
β/ deg	90.00	91.69 (1)
V/Å^3	823.5 (2)	1013.0 (2)
D_x/g cm^{-3}	1.357	1.339
F(000)	360	440
μ/mm^{-1}	0.0895	0.101
Data Collection		
Cryostat	He/closed cycle	
λ/Å	0.71073	
$(\sin\theta/\lambda)_{max}$	1.15	
Scan technique	$\omega/2\theta$	
Diffractometer	Syntex P1bar	Siemens P4
Scan speed (2θ)/deg min^{-1}	4	3
No. collected reflections	24625	13171
No. unique reflns	5163	5535
No. observedd reflections (I > 0, N_{obs})	4761	5374
Multipolar refinement (VALRAY)		
Refinement Results on all data		
GoF	1.2462	0.7169
R(F), R (F^2)	0.0233, 0.0217	0.0212, 0.0210
R$_w$ (F^2)	0.0326	0.0296
No. variables (N_v)	212	508
N_{obs}/N_v	22.5	10.6
On data within the Cu sphere		
No.obs reflns (I > 0)	927	2225
R (F), R (F^2)	0.0107, 0.0189	0.0146, 0.0147
R$_w$ (F^2)	0.0209	0.0203

2.3. Multipolar Refinement

For the full-matrix least-squares refinement of the SQ and SQDH low-T structures, multipolar scattering factors were used as implemented in the VALRAY code [27–29], to model the asphericities in the electron density distribution [21]. The corresponding pseudo-atom models included, for both crystals, multipoles up to the octupole level for the C, N and O atoms and to the quadrupole level for the H atoms. Positional parameters of the latter atoms were evaluated with the "polarized H atoms" option of VALRAY, and their anisotropic U_{ij}'s were estimated (and not refined) with the ADPH code of Roversi and Destro [21]. The results of the refinements are summarised in Table 2 [30]. The analysis of the experimental $\rho(\mathbf{r})$ in terms of topological features, nuclear-centred distributed multipole analyses (DMA) and derived electrostatic properties was carried out both with VALRAY and by means of the program PAMoC (an acronym for properties of atoms and molecules in molecular crystals) [21], which retrieves all the required information from the binary checkpoint file produced by VALRAY [31].

3. Results and Discussion

3.1. The Structures

The atomic numbering scheme adopted for the asymmetric units of the two compounds is illustrated in Figure 2, and the crystal packings for the two structures are shown in Figure 3. The previously published numbering scheme has been maintained for the C and H atoms of SQ [9], while for SQDH the atomic labels of reference have been redefined (eliminating the need for "A" and "B" labels) [11].
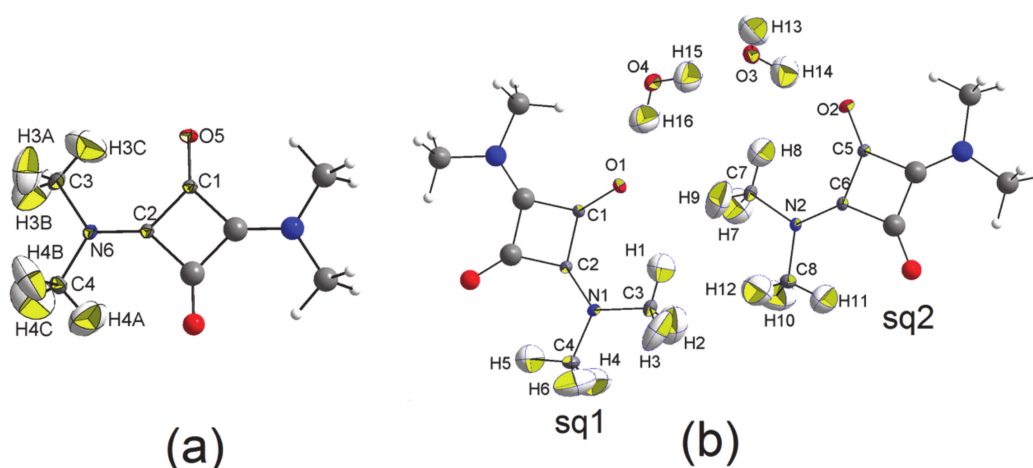

Figure 2. (**a**) SQ at T = 18 (1) K, with symmetry-independent atoms belonging to the asymmetric unit labelled with their numbering scheme. Thermal ellipsoids were drawn (also for the asymmetric unit only) at the 90% probability level. Anisotropic thermal ellipsoids of H atoms were estimated by the ADPH program [30]. (**b**) Same as (**a**) for SQDH at T = 20 (1) K. The two symmetry-independent molecules are labelled as "sq1" and "sq2" (see text).
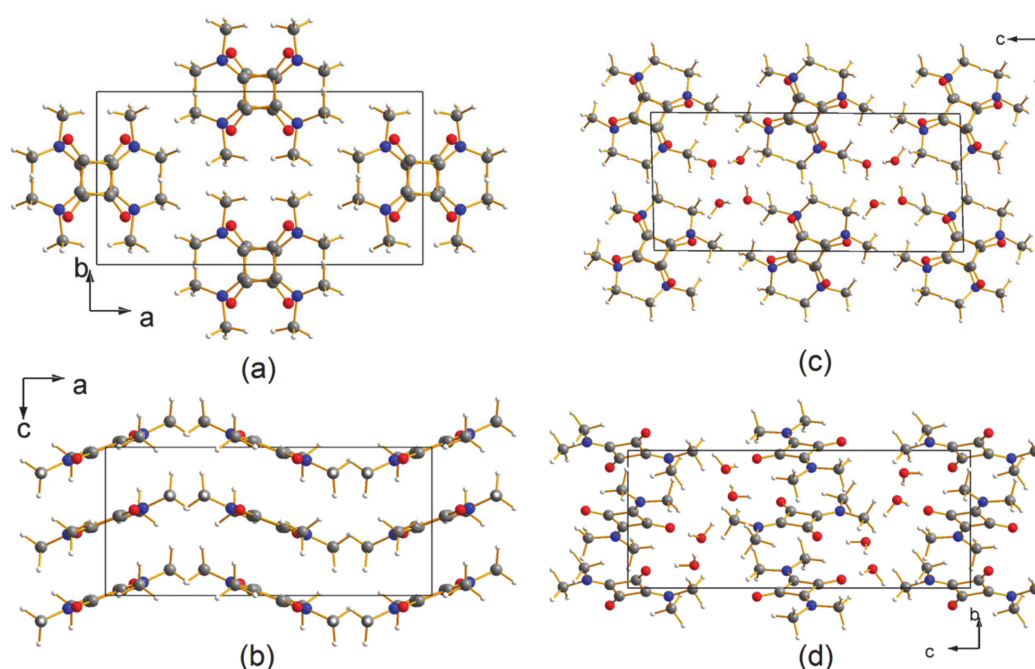
Figure 3. (**a**) Crystal packing of SQ at T = 18(1) K, as seen along the *c* axis. The atoms have the usual color code; grey: C; white: H; red: O; blue: N). (**b**) Same as (**a**), along *b*. (**c**) Crystal packing of SQDH at T = 20(1) K viewed down the *b* axis. (**d**) Same as (**c**), along *a*.

As seen in Figure 3a,c, the molecules are arranged in stacks in both crystals, with neighbouring molecules along the stacks almost orthogonal to each other, the angle between their longest inertia axes amounting to about 100 deg in SQ and about 93 deg in SQDH. This implies that C=O and C-N bonds of stacked molecules are almost parallel, with negatively charged O and N atoms (see below) close to each other. Clearly, crystal packing is not dominated just by attractive interactions of net point charges, but it likely stems from the interplay of high-order electrostatic terms, and dispersive–repulsive Lennard–Jones contributions. The cohesive energy analysis goes beyond the purpose of this work and could be the topic of further studies. In any case, the orientation of the molecules with respect to the cell axes is very different in the two structures. Indeed, the projections of the longest inertia axes of the *crystallographically (hence structurally) equivalent* alternating squaraines of SQ on the plane perpendicular to the stacking direction both form an angle of about 40 deg with the long *a* axis, while those of the *structurally different* alternating squaraines of SQDH make angles of 23 deg and 70 deg with *c*, the cell long axis of the dihydrated crystal. In other words, compared with the anhydrous crystal, one squaraine appears to be rotated clockwise by 17 deg and the other by 30 deg. Figure 3b,d show that the molecular planes of SQ along the stacks are parallel to each other and virtually parallel to the *b* axis; these planes are tilted by 21.3 deg, as measured by the angle formed by the normal to the planes and the direction of the stack (i.e., the cell *c* axis). In SQDH, the molecular planes are tilted by about 26 deg with respect to the stacking *b* axis and almost parallel to the longest cell axis *c*, since the normal to the plane of one squaraine makes an angle of 89.4 deg with this axis, and the normal of the other plane an angle of 84.5 deg. Owing to the reduction of the cell axes lengths in the stacking direction on going from RT to low T (see Figure 1), the distances between the centres of mass of the squaraine molecules along the stacks decrease from 3.493 Å to 3.420 Å in SQ, and from 3.742 Å to 3.577 Å in SQDH, that is by a double amount in the dihydrate.

This different behavior, as well as the large difference between the overall molecular arrangements of the two crystals, is likely related to the presence, in SQDH, of columns of water molecules spiraling around the screw axes (see Figure 4), with each column involved in intermolecular interactions with the four surrounding squaraine molecules, each belonging to different pillars of translation-related

stacked units. It is the inclusion of water molecules that completely modifies the overall packing observed in SQ.
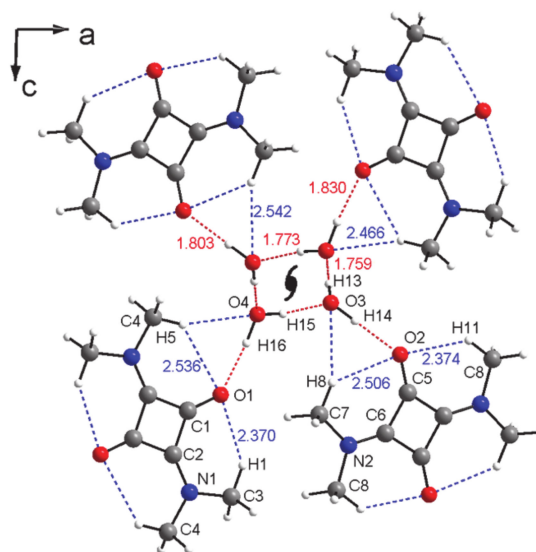

Figure 4. View of the main hydrogen bond (HB) motifs along the monoclinic *b* axis of SQDH at T = 20(1) K. Co-crystallized water molecules fold around the 2_1 axis, forming strong OH···O HBs (dashed red lines) with keto groups in squaraine. Both intramolecular and intermolecular weaker CH···O bonds (dashed blue lines) are also set up. Independent HB distances are shown.

As for the molecular geometries, we note that the corresponding bond distances and angles involving non-H atoms of the two independent squaraine molecules in SQDH (hereinafter sq1 and sq2) are in very close agreement. The largest difference in bond distances amounts to a mere 0.003Å (~15 esds), and is observed at the N-C_{ring} bond, while bond angles do not differ by more than 0.5 deg. More relevant is the deviation from *mmm* symmetry in both SQDH molecules: labelling as Cα the C atom bonded to the squaraine O atom, and as Cβ the other ring C atom, the O-C_α-C_β angles (that is, O1-C1-C2 in sq1 and O2-C5-C6 in sq2) differ by more than 2 deg in sq1 and by 1.39 deg in sq2, and differences larger than 1 deg (1.29 deg and 1.05 deg) are observed at the C_{ring}-N-C_{methyl} angles. The two pairs of angles external to the ring at the C atom bonded to the dimethylamino group also differ significantly, by 1.91 deg in the sq1 pair and 1.41 deg in the sq2 one. The deviation of the squaraine from *mm2* symmetry is much smaller in SQ, where the difference between the two C_{ring}-N-C_{methyl} angles is 0.95 deg, while that at the other two pairs of angles discussed above is less than 0.4 deg (0.38 deg for the pair involving the O-C bond and 0.32 deg for the remaining pair). We may infer that the presence of columns of water molecules in SQDH, and hence the different network of intermolecular interactions with respect to that of SQ, results in a deformation, however modest, of the average structure of the squaraine molecule.

Indeed, as seen in Figure 4, the new further contacts between the squaraine atoms of SQDH and the water molecules is accompanied by a noticeable variation in the lengths of the two intramolecular O···.H contacts in each molecule with respect to the two values, 2.401 and 2.456 Å, observed in SQ. Full lists of the shortest (<3.1 Å) O···H distances in the two compounds are reported in Tables 3 and 4, while Table 5 reports the contacts of the water molecules of SQDH with the O and H atoms of the contiguous squaraines.

Table 3. Short (<3.1 Å) non-equivalent O···H contacts [a] of atom O5 in SQ.

O···H-C	$d_{O···H}$ (Å)	Angle OHC (deg)	Position of CH Atom
		Intramolecular	
O5···H3C-C3	2.401	136.35	x, y, z
O5···H4A-C4	2.456	133.86	1 − x, −y, −z
		Intermolecular	
O5···H4C-C4	2.487	130.56	1 − x, y, −$\frac{1}{2}$ − z
O5···H4B-C4	2.561	149.44	$\frac{1}{2}$ + x, $\frac{1}{2}$ − y, −z
O5···H3B-C3	2.928	123.36	1 − x, y, −$\frac{1}{2}$ − z
O5···H3B-C3	3.017	95.70	1 − x, 1 − y, −z

[a] Estimated standard deviations (esds) are <0.001 Å for the distances *d* and <0.01 deg for the angles.

Table 4. Short contacts [a] of the two half-squaraines O atoms with the methyl H atoms in SQDH.

O···H-C	$d_{O···H}$ (Å)	Angle OHC (deg)	Position of CH Atoms
		Intramolecular	
O1···H1-C3	2.370	135.08	x, y, z
O1···H5-C4	2.536	131.30	−x, −y, −z
O2···H8-C7	2.506	132.56	x, y, z
O2···H11-C8	2.374	135.11	−x, 1 − y, −z
		Intermolecular	
O1···H7-C7	2.465	141.66	−x, −y, −z
O1···H9-C7	2.759	114.63	1 + x, y, z
O1···H10-C8	2.885	131.68	−x, −y, −z
O2···H3-C3	2.741	122.29	−x, 1 − y, −z
O2···H6-C4	2.920	113.53	x, $\frac{1}{2}$ − y, −$\frac{1}{2}$ + z
O2···H5-C4	3.033	100.31	−x, −y, −z

[a] *d* < 3. 1 Å; esds are <0.001Å for *d*'s and ≤0.02 deg for angles.

Table 5. Short [a] water contacts [b] in SQDH.

O···H-O or O···H-C	$d_{O···H}$ (Å)	Angle OHO (deg) or Angle OHC	Position of CH (or OH) Atoms
		Water···water	
O3···H15-O4	1.772	169.32	x, y, z
O4···H13-O3	1.759	178.42	1 − x, −$\frac{1}{2}$ + y, −$\frac{1}{2}$ − z
		Water···O$_{squaraine}$	
O1···H16-O4	1.830	169.44	x, y, z
O2···H14-O3	1.803	179.02	−1 + x, y, z
		Water···H$_{methyl}$	
O3···H8-C7	2.542	156.87	1 + x, y, z
O3···H4-C4	2.660	146.27	1 − x, −y, −z
O4···H2-C3	2.630	167.08	1 − x, −y, −z
O4···H5-C4	2.466	156.15	−x, −y, −z
O4···H3-C3	2.680	131.16	x, $\frac{1}{2}$ − y, −$\frac{1}{2}$ + z

[a] Distances (Å) less than the sum of van der Waals radii, 1.5 for O and 1.2 for H atoms. [b] Esds as in Table 4.

Of the six unique O···H contacts of each O atom in SQ (Table 3), two are intramolecular, two are intracolumnar, and the remaining two connect one stack to two different columns (Figure 3). The number of short O···H interactions for each of the two half-squaraine molecules of SQDH is the same (six), but the pattern is partly different: in sq1 the oxygen atom O1 is involved in two

intramolecular interactions, as in SQ, but here the intracolumnar contacts are three (see Table 4), and the sixth interaction is the only inter-stack contact, 1.830 Å long, that is a strong H-bond with the water molecule at O4 (see also Table 5 and Figure 4). Similarly, the oxygen atom O2 of sq2 shows two intramolecular and three intracolumnar contacts with methyl C-H groups, and one H-bond with the other water molecule including O3. The relevance or otherwise of this difference between SQ and SQDH will be evident when the electron distribution of the two crystals will be analysed

An interesting feature of the packing in both crystals is the presence of short distances, well below 3.4 Å (the latter distance being twice the C atom van der Waals radius) between ring C atoms of superimposed squaraine molecules along the columnar stacks. In SQ, the atom C1 is only 3.168 Å away from its symmetry-related mate at $1 - x$, y, $\frac{1}{2} - z$, and in SQDH the corresponding pair is separated by 3.196 Å. For the other C atom of the ring of SQ, that is atom C2, the analogous separation, 3.271 Å, is slightly larger, but still short, while a distance of only 0.057 Å less than 3.4 Å is observed for the related pair in SQDH.

Finally, we looked at the planarity of the squaraine molecules in the two crystals. The twelve non-H atoms of the molecule in SQ are all coplanar within ±0.054 Å (plane A). If the four methyl C atoms are excluded from the calculation of the least-squares plane, the coplanarity of the other eight atoms is within ±0.004 Å (plane B). Distances from this plane for the four H atoms pointing towards the O atoms are 0.098 Å for atoms H4A and its centrosymmetric mate (on opposite sides), and 0.136 Å for the other pair formed by atom H3C and its mate. The two squaraines of SQDH are slightly more planar, with distances within ±0.019 Å and ±0.038 Å for the 12 atoms of the corresponding planes A of sq1 and sq2, respectively. The eight atoms of planes B are within ±0.005 Å in sq1 and within ±0.002 Å in sq2. The distances from these planes for the H atoms of sq1 and sq2 corresponding to atoms H4A and H3C of SQ amount to 0.110 Å and 0.127 Å in sq1, which are reduced to 0.046 Å and 0.076 Å in sq2.

In summary, a substantial similarity is expected, on pure geometric grounds, for the main features of the charge density distribution in the intramolecular space of SQ and SQDH squaraines. As it is well known that geometric parameters are not sufficient to characterize the C-H⋯O contacts as hydrogen bonds or van der Waals interactions, an accurate topological analysis of the distribution of the electrons in the space between the C-H group and the oxygen atom is necessary [32–36]. The results of this analysis for SQ and SQDH will be described in the next section.

3.2. The Electron Density Distribution (EDD)

Experimental electron density distributions (EDDs) for the two crystals were derived from least-squares refined multipolar models. Each EDD was topologically analysed by means of the appropriate routines of the PAMoC [31] and VALRAY [21] software programs. A previous paper on DMACB (the 1,2 substituted isomer of SQ) summarises the EDD topological analysis [34], originally devised for theoretical charge densities, but then widely applied to experimental electron distributions [37] (for very recent applications see refs. [38,39]). Selected values of $\rho(\mathbf{r})$ and its Laplacian $\nabla^2\rho(\mathbf{r})$ at the (3, −1) bond critical points (bcps) of the squaraine molecules are listed in Table 6.

Table 6. Properties [a] of the charge density $\rho(\mathbf{r}_b)$ (eÅ^{-3}) and the Laplacian $\nabla^2\rho(\mathbf{r}_b)$ (eÅ^{-5}) at the (3, −1) bcps of the chemical bonds (Å) and intramolecular O⋯H contacts (Å) of the squaraine molecules in the SQ and SQDH crystals.

| | SQ | | | SQDH | | | | | | | |
| | | | | Sq1 | | | | Sq2 | | | |
Bond	Length b. path	$\rho(\mathbf{r}_b)$	$\nabla^2\rho(\mathbf{r}_b)$	Bond	Length b. path	$\rho(\mathbf{r}_b)$	$\nabla^2\rho(\mathbf{r}_b)$	Bond	length b. path	$\rho(\mathbf{r}_b)$	$\nabla^2\rho(\mathbf{r}_b)$
O5-C1	1.237 1.237	2.85(1)	−36.2(6)	O1-C1	1.241 1.241	2.82(2)	−33(1)	O2–C5	1.239 1.239	2.87(2)	−34(1)
C1-C2	1.467 1.473	1.844(8)	−12.1(2)	C1-C2	1.467 1.472	1.81(1)	−10.2(3)	C5–C6	1.466 1.472	1.82(1)	−10.6(3)
C1-C2′	1.467 1.472	1.845(8)	−12.1(2)	C1-C2′	1.466 1.470	1.82(1)	−10.7(3)	C5–C6′	1.465 1.469	1.80(1)	−10.3(3)

Table 6. *Cont.*

SQ				SQDH							
				Sq1				**Sq2**			
C2-N6	1.318 1.318	2.48(1)	−29.8(5)	C2-N1	1.316 1.316	2.47(2)	−25.7(6)	C6–N2	1.319 1.319	2.48(2)	−25.2(6)
N6-C3	1.457 1.457	1.74(1)	−10.5(3)	N1-C3	1.462 1.462	1.70(1)	−8.2(5)	N2–C7	1.462 1.462	1.72(1)	−8.7(5)
N6-C4	1.458 1.458	1.77(1)	−10.9(3)	N1-C4	1.461 1.462	1.72(1)	−8.5(5)	N2–C8	1.463 1.463	1.70(1)	−7.9(5)
C3-H3A	1.080 1.081	1.92(2)	−17.5(6)	C3-H1	1.072 1.072	1.92(2)	−17.4(8)	C7–H7	1.088 1.088	1.99(2)	−20.0(8)
C3-H3B	1.087 1.088	1.90(2)	−17.9(6)	C3-H2	1.100 1.101	1.88(2)	−15.9(9)	C7–H8	1.078 1.079	1.90(2)	−16.3(9)
C3-H3C	1.062 1.063	1.91(2)	−17.2(9)	C3-H3	1.092 1.092	1.94(2)	−18(1)	C7–H9	1.089 1.090	1.97(2)	−19.2(8)
C4-H4A	1.063 1.063	1.96(2)	−19.0(6)	C4-H4	1.062 1.063	1.90(2)	−16(1)	C8–H10	1.106 1.107	1.92(2)	−18.0(8)
C4-H4B	1.073 1.074	1.98(2)	−20.2(6)	C4-H5	1.089 1.089	1.85(2)	−14.8(8)	C8–H11	1.078 1.079	1.94(2)	−17.2(9)
C4-H4C	1.115 1.115	1.91(1)	−17.8(5)	C4-H6	1.076 1.077	1.85(3)	−14(1)	C8–H12	1.091 1.092	1.91(2)	−16.4(8)
Intramolecular contacts											
Contact	Distance b. path	$\rho(r_b)$	$\nabla^2\rho(r_b)$	Contact	distance b. path	$\rho(r_b)$	$\nabla^2\rho(r_b)$	Contact	distance b. path	$\rho(r_b)$	$\nabla^2\rho(r_b)$
O5···H3C	2.401 2.413	0.070(2)	1.03(1)	O1···H1	2.370 2.397	0.082(3)	1.09(1)	O2···H11′	2.374 2.413	0.078(3)	1.08(1)
O5···H4A	2.456 2.464	0.061(1)	0.91(1)	O1···H5′	2.536	Not found		O2···H8	2.506	Not found	

[a] Estimated standard deviations (esds) for bond lengths are <0.001Å.

From the overall topological analyses of the experimental EDDs of the two crystals, the following features are worth discussing:

(i) In all three squaraine molecules, the lengths of the bond paths are very close to the related interatomic distances, except for the two independent bent bonds of the squarylium rings, where the numerical values of the bond paths differ significantly from the geometric distances (e.g., Δs = +0.0054 Å and +0.0051 Å in SQ, see Table 6). Longer bond path lengths are due to bond bending, as found in other 4-membered rings. In SQ, the two lines (bond path and bond length) make angles of 4.5 deg and 4.9 deg at the C atom bonded to the O atom [40,41], and of 5.7 deg and 5.9 deg at the other C atom, bonded to the N atom. Similar values—in the range 3.5 deg–6.7 deg for sq1 and 4.0 deg–5.5 deg for sq2—are observed at the corresponding angles of the squaraine rings of SQDH.

(ii) There is a larger accumulation of charge on the ring C-C bonds of SQ than in those of sq1 and sq2 in SQDH: the values of $\rho(r_b)$ at the bcps of the former bonds are greater than those in the dihydrated crystal by 2.4–4.5 times the larger esds, and the values of the corresponding Laplacians differ by more than 5–6 times the esds of sq1 and sq2.

(iii) The same features are shown by the N-C$_{methyl}$ bonds: the values of $\rho(r_b)$ at the bcps of these bonds in SQ are larger, on average, by 0.045 eÅ^{-3} (i.e., 4.5 esds) than those of sq1 and sq2, and their $\nabla^2\rho(r_b)$ quantities are more negative by ca. 2.4 eÅ^{-5} (again more than 4 esds). Differences of 4.1 and 4.6 eÅ^{-5} are observed also at the Laplacian of the (3, −1) bcp of the other N-C bond, whose length indicates a significant amount of double bond character in all three squaraine molecules. This statement is confirmed also by the value of $\rho(r_b)$ at the latter bond, 2.48 eÅ^{-3}, only marginally smaller than that (2.51 eÅ^{-3}) we found [42] at the bcp of the formally pure N = C double bond, 1.332 Å long, of a thiazete compound at T = 100(2) K.

(iv) For a complete isolated molecule of SQ (hence for a whole of two asymmetric units) the total number of (3, −1) bond critical points we found is 28, including 24 points for the 24 chemical bonds and 4 points for the four intra-molecular O···H interactions (Table 6). There are five (3, +1) ring critical points (rcps), corresponding to the squarylium ring plus the four six-membered

rings formed by the sequence O-C_α-C_β-N-C_{methyl}-H_{methyl}. With 24 attractors (the 24 atoms of the molecule) and no (3, +3) cage critical points, the Morse relation [43] is satisfied. The full corresponding set of atoms in SQDH includes two complete squaraine molecules (sq1 and sq2) plus two water molecules, for a total of 54 attractors. For this system, the Morse condition is also fulfilled: we found 61 bcps and 8 rcps. However, at odds with SQ, there are only two intramolecular O···H bond paths per sq molecule instead of four. As reported at the bottom of Table 6, no interaction lines were found for two of the O···H contacts and their centrosymmetric mates. Rather, each of the two H atoms no longer bonded to the squaraine O atom is now connected by a bond path to a water O atom (see Figure 4), and two eight-membered rings are formed, since each water molecule has one of its H atoms connected to the squaraine O atom. As a result, SQ and SQDH show different topologies of the squaraine molecules, in spite of the substantial geometric similarities described above.

When theoretical EDDs are compared to experimental results, it is often said, correctly, that the former are mostly affected by the choice of quantum mechanical method, the latter by quality of the sample, treatment of the data, and choice of multipolar model (to cite only a few sources of error). In all our EDD studies so far (starting with the one of crystalline citrinin at 19 K) [44], we have found that reliable modelling of H atoms requires anisotropic displacement parameters (ADPs), and poles up to the quadrupole level [45,46].

This study is no exception: as shown in Figure 5, expansion of the H electron density up to quadrupole level is necessary to correctly model intramolecular O···H bonds. The case reported in the Figure is that of the squaraine molecule of SQ. Figure 5a shows the contour plot of the electron density drawn after the refinement of a model for the H atoms with ADPs and poles only up to the dipole level: there is no indication as to the intramolecular O···H bcps. Figure 5b illustrates the electron density in the same region of the SQ crystal, after inclusion of the quadrupole terms in the H pseudoatoms: the expected saddle shape of the contours in the O···H bonds clearly shows up.

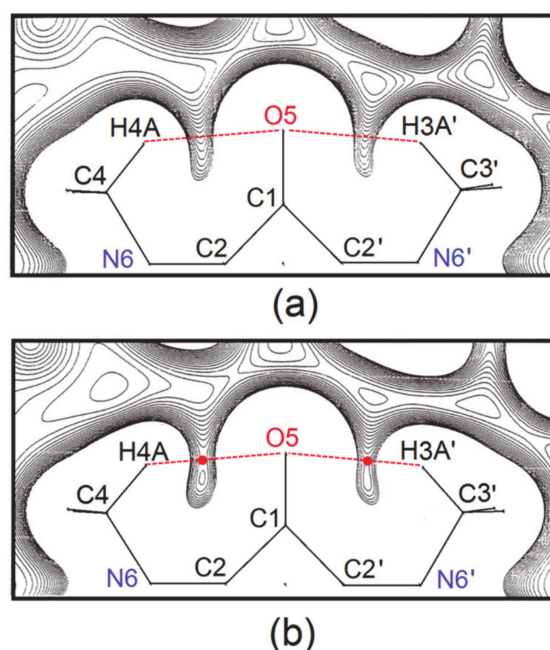**Figure 5.** Total experimental charge density of SQ at T = 18(1) K in the main molecular plane. Level lines are drawn at steps of 0.01 e·Å^{-3}. (**a**) The multipole expansion includes poles up to $l = 1$ for hydrogen atoms: neither H4A···O5 nor H3A'···O5 atomic interaction lines are present. (**b**) Same as (**a**), with $l = 2$ poles included on hydrogens. Now, (3, −1) saddle points are clearly detectable in the $\rho(\mathbf{r})$ scalar field (red dots). Dashed red lines serve just as guides for the eye, to highlight relevant non-covalent interactions.

Figure 6 shows the total charge density and the corresponding Laplacian distribution of the sq2 squaraine molecule in SQDH. Maps for the sq1 molecule are essentially identical. Local anisotropy of EDD around each atom can be appreciated. Hydrogens H8 and H11 are clearly oriented towards the two valence shell charge concentration (VSCC) regions of the O2 basin, corresponding to the oxygen lone pairs (Figure 6b). These interactions are dominated by a large region of charge depletion, in agreement with the expected main electrostatic character. As expected from the resonant character of the four-membered ring [9,47], the N2-C6 and O2-C5 bonds have both a significant double bond degree (see also Table 6). Accordingly, the C-C distances bear a larger σ character, as there is one resonant double bond delocalized over four ring edges.
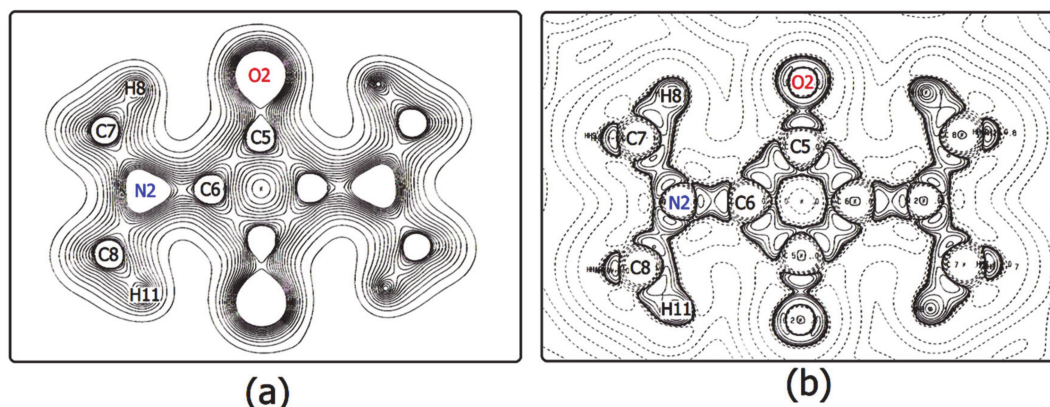

Figure 6. (**a**) Total experimental charge density of SQDH (molecule sq2) at T = 20(1) K in the main molecular plane. Level lines are drawn at steps of 0.01 e $Å^{-3}$. (**b**) Distribution of $-\nabla^2\rho(\mathbf{r})$ at variable-step ($\pm a \cdot 10^{-n}$ e/A^5, with a = 9.64, 4.82 and 2.20 and n = 0, ±1, ±2, ±3, ±4 and ±5). Full lines mark isovalues where electronic charge is locally concentrated, while dashed lines highlight isovalues where charge is locally depleted.

3.3. The Electrostatic Potential

Maps of the electrostatic potential $\Phi(\mathbf{r})$, plotted in units of e $Å^{-1}$, were calculated for the squaraine molecules extracted from the crystals, that is considering only the contributions of the pseudoatoms of one molecule. We recall that this pseudoatom potential is not the same as that of an isolated molecule in the gas phase, because the charge density distribution is altered by the crystal environment.

A 2D contour plot (perhaps old-fashioned, but still useful and informative) of the molecular $\Phi(\mathbf{r})$ for the squaraine molecule of SQ, calculated in the plane of the central four-membered ring, is reported in Figure 7a, which clearly illustrates the quadrupolar nature of the 1,3-bis(dimethylamino)squaraine. The map of Figure 7a is computed from a model with isotropic thermal displacement parameters for H atoms. The minimum in this map amounts to −137 ± 19 kJ mol^{-1}, about 1.345 Å away from the oxygen atom. Upon addition of anisotropic U_{ij}'s and quadrupolar terms added to the H pseudoatoms, the minimum is −184 ± 17 kJ mol^{-1}, and closer to the O atom, only 1.253 Å away. Oxygen atoms completely dominate the nucleophile region of the molecule, as it can be appreciated also in the map of Figure 7b, where a section of $\Phi(\mathbf{r})$ in the plane perpendicular to that of Figure 7a, and passing through the midpoints of two opposite bonds of the squarylium ring, shows a minimum of −129 ± 19 kJ mol^{-1} at 1.712 Å from the centre of the ring and 2.845 Å from one oxygen atom and 2.872 Å from the other. Addition of anisotropic U_{ij}'s and quadrupolar terms to the H pseudoatoms reduces the same minimum to −28 ± 17 kJ mol^{-1}, at a position 2.308 Å from the centre of the molecule, 3.190 Å from an O atom and 3.209Å from the other one.
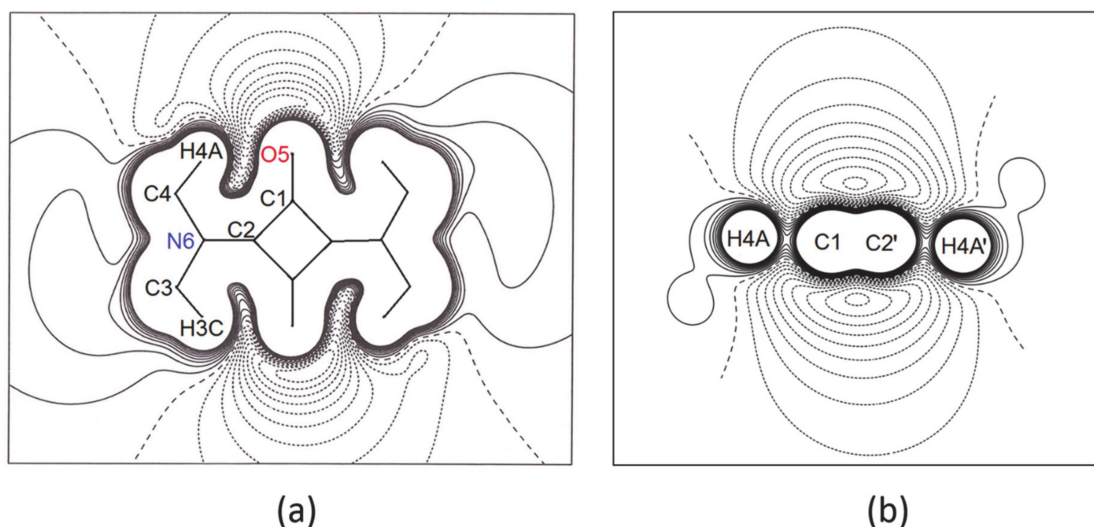
(a)　　　　　　　　　　　　　　　　　　　　　(b)

Figure 7. (**a**) Experimental electrostatic potential Φ(**r**) of SQ in the mean molecular plane, extracted from the crystal, as computed from a model with isotropic H atoms. Contour levels run from −0.09 to +0.09 e·Å^{-1} at steps of 0.01 e·Å^{-1} (1 e Å^{-1} = 1389 kJ·mol^{-1} = 14.4 V). All the atoms within 0.1 Å from the plane are shown. (**b**) Same as (**a**), plotted in the perpendicular plane passing through the C1–C2 and C1′–C2′ midpoints Negative and zero contours: short and long dashed lines, respectively; positive contours: solid lines.
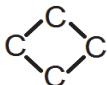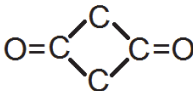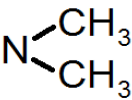
The striking difference of the electrostatic potential above the ring, that is in a region where non-H atoms play a major role in determining properties, makes it clear that the variations induced in the modelling of H atoms have significant consequences in regions far from these nuclei.

The essential features of Φ(**r**) in the plane of the squarylium rings of sq1 and sq2 in SQDH do not differ significantly from those of Figure 7, but the minima of Φ are significantly reduced, amounting to −139 ± 13 kJ mol^{-1} in the plane of sq1 and to −137 ± 13 kJ mol^{-1} in that of sq2. The distances of the Φ minima from the closest O atoms is about the same in both planes, 1.241 Å for sq1 and 1.249 Å for sq2. The reduction in the Φ values in SQDH is not due to a different model for the H pseudoatoms of the dihydrate with respect to that of the anhydrous crystal, because U_{ij}'s were derived with the same procedure and a quadrupolar expansion was used on both models. Rather, it seems to indicate that the SQDH EDD is modified to a significant extent by the presence of the water molecules, ΔΦ being three times the pooled standard deviation. Further clues to the reasons for the differences in the electrostatic potential of the squaraine molecules in the two crystals may be obtained from a close inspection of the atomic or group charges, as described below.

3.4. Atomic Volumes

Bader's Quantum Theory of Atoms in Molecules (QTAIM) [37] was applied to both crystals to partition their experimental EDDs into atomic basins, and hence to obtain, by integration, atomic volumes and charges. The calculations were made with the PAMoC code. Since these basin properties are additive [31], a useful comparison among the three squaraine molecules can be made by comparing the values of equivalent molecular fragments (Table 7).

Table 7. Experimental Group Volumes (Å^3) of the squaraine molecules in SQ and SQDH crystals from QTAIM partitioning of the electron density. [a] Esds on the last significant digit are reported in parentheses.

Group	SQ	SQDH	
		Squaraine #1	Squaraine #2
(four-C ring)	35.50(2)	35.95(2)	35.88(2)
$O=C$ ... $C=O$ (ring)	70.32(2)	70.29(2)	69.94(2)
CH_3	29.4(1)	29.5(3)	29.4(3)
N(CH_3)(CH_3)	70.6(1)	70.4(4)	70.4(4)
molecule	211.5(2)	211.1(5)	210.7(5)

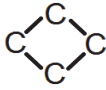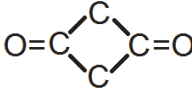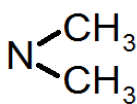[a] For the methyl groups, the average value in each molecule is reported.

It can be seen that the average volumes of the methyl groups and those of the bis-dimethylamino fragments are the same in all three molecules, with no difference exceeding one corresponding pooled standard deviation. The central portion of the molecules, that is the four-C ring plus the two oxygen atoms, has the same volume in SQ and in the squaraine sq1 of SQDH, while that group volume in sq2 is smaller than that in SQ by 0.38 ± 0.02 Å^3. The volumes of the squarylium rings of the same two molecules differ by roughly the same amount—but now the larger value is that of sq2. It is the volume of the two O atoms that is larger by 0.76 ± 0.01 Å^3 in the anhydrous crystal than in molecule sq2, while the volume of these two atoms in sq1 exceeds that in sq2 by 0.28 ± 1 Å^3, but is smaller than that in SQ by 0.48 ± 1 Å^3. Both crystallographically independent four-membered rings in the SQDH crystal occupy a significantly larger volume than that in the anhydrous compound molecule (Δs of 0.45 ± 0.02 and 0.38 ± 0.02 Å^3, respectively, for sq1 and sq2).

As for the water molecules in SQDH, from the values of the crystallographic cell volumes (see Table 1) of the two crystals, one would expect an average volume of 23.69 Å^3 per H_2O molecule. The QTAIM average volume is 5% larger, 24.94 Å^3, but the two individual H_2O volumes, 27.06(2) Å^3 and 22.81 Å^3, differ by more than 15% of the value of the larger V_{H2O} (i.e., the H_2O containing O3). It can be seen from Figure 4 that this water molecule is linked, through a hydrogen bond, to the sq2 squaraine molecule, as well as to the other water molecule. This observation should be remembered when dealing with the charges of the two molecules.

3.5. Atomic Charges

The observed differences in atomic volumes between the two crystals anticipate substantial differences also between atomic charges. The group charges are listed in Table 8. Like the volumes, the charges of the methyl groups show the same value in the three molecules, but the same is not true of the bis-dimethylamino fragments. In particular, the N atom of SQ carries a charge of $-0.95e$, while those of sq1 and sq2 have charges of $-0.85e$ and $-0.83e$, respectively. The standard deviations estimated by PAMoC [31] for these quantities are $0.008e$ in SQ and $0.01e$ in SQDH. Therefore, in terms of esds the differences in integrated charges at the N atoms are significant across the two crystal forms.

Table 8. Experimental Group Charges (electrons) of the squaraine molecules in SQ and SQDH crystals from QTAIM partitioning of the electron density. [a] Esds on the last significant digit are in parentheses.

Group	SQ	SQDH	
		Squaraine #1	Squaraine #2
(ring of four C atoms)	2.39(1)	2.16(2)	2.18(2)
$O=C$ ... $C=O$ (ring with two C=O)	0.42(2)	0.32(2)	0.32(2)
CH_3	0.37(3)	0.35(2)	0.37(2)
$N(CH_3)_2$	−0.21(4)	−0.15(3)	−0.09(3)
molecule	0.00(6)	+0.02(5)	+0.14(6)

[a] As in Table 7, for the methyl groups the average value in each molecule is reported.

The excess of electronic population on N and O atoms, as well as the strongly positively charged squarylium ring (Table 8), mirrors a larger weight of the σ resonance form, where positive charges are preferentially located on the N-bonded C atoms of the ring. However, other resonance forms, which invariably imply an extended degree of conjugation between N and O atoms through the C backbone, are not negligible. For example, N-C and C-C bond lengths (Table 6) are consistent with some degree of π character in the squaraine core structure. In keeping with the differences observed in the charges on N atoms, significant differences are also apparent in the charges of the squarylium rings and of those of the central molecular fragment (ring plus two O atoms). The sq1 and sq2 molecules have the same charge value at the central fragment, and very similar values at the ring, but the corresponding values in the squaraine molecule of SQ differ, the Δs being five times the esd at the central fragment and as large as 0.23e and 0.21e (more than 10 esds) at the ring.

The sum of all atomic charges (last row of Table 8) qualifies the molecule of SQ as perfectly neutral, and molecule sq1 as practically neutral (in terms of the corresponding esd). The sq2 molecule appears instead positively charged, but the relatively large esd suggests that the estimated value must be assessed with caution. As for the water molecules of SQDH, we first recall that the two distinct molecules are linked to each other by strong H-bonds with O···H separations of 1.772 Å and 1.759 Å (Table 5 and Figure 4). Furthermore, each of them is also involved in two other H-bonds with a single squaraine molecule, i.e., the water at O3 with sq2 and the other H_2O molecule (at O4) with sq1 (see Figure 4). The integration process by PAMoC [31] gives the H_2O at O3 a negative charge of −0.15 ± 0.02e, which slightly exceeds, with opposite sign, the total charge of +0.14 ± 0.06e of sq2, bonded to it through a short H-bond 1.803 Å long. The small excess of negative charge can partly compensate for the positive charge (+0.06 ± 0.01e) of the other water molecule, which is in turn hydrogen-bonded to the virtually neutral squaraine sq1 by a H-bond that is 1.830 Å long. The large difference of about 0.20e between the total charges of the two water molecules is mostly due to the charge difference between the two pairs of H atoms (Δ = 0.145e), with a difference of about 0.06e for the two O atoms, the O3 atom being the most negative (q = −0.978 ± 0.008e) of the entire system.

The total charge for a cluster of two squaraine molecules and four water molecules, hence half the content of the crystallographic cell of SQDH, differs from zero by 0.02e, owing to the choice of reporting charge values rounded off at the last significant digit. This quantity can be taken as a measure of the overall accuracy of our evaluation of this electrostatic property in the dihydrated compound. Overall, the SQDH structure can be described as a central column of spiraling water molecules acting as a polymeric anion surrounded by alternating columns of positively charged squaraine molecules.

This picture suggests an intermolecular charge transfer (ICT) between squaraine and water molecules, not dissimilar to the one [48] observed from small squaraines to ZnO nanoparticles, a process that the authors of that study predict might increase the performance of solar cells. ICT between tightly packed squaraine molecules has also been shown [49] to have a major influence on the optical and electronic properties of squaraine multimers, and has been invoked to explain the origin and nature of the absorption spectra of these systems.

3.6. Molecular Electrostatic Moments

Electrostatic moments compactly represent the main characteristics of the molecular EDD [50], and can be calculated with great accuracy from accurate XRD-derived charge densities. [51] The usefulness of multipolar moments to reveal molecular similarities and differences is well documented, but their values are rarely reported in the literature [52,53], although the misconceptions that have limited their use have already been clearly refuted some time ago [54].

For the squaraine molecules of the present study, only quadrupole moments can be evaluated, because the three molecules are located at crystallographic centres of symmetry, and therefore dipole and octupole moments are necessarily null. No such restriction holds for the SQDH water molecules, whose dipole moments can be evaluated. The PAMoC code derived the components of the dipole vectors and those of the quadrupole tensors from two distinct distributed multipole analyses (DMA), one based on the population parameters of Stewart's pseudoatoms (i.e., obtained from the least-squares structure refinement) the other based on Bader's QTAIM. PAMoC calls these analyses as Stewart DMA and QTAIM DMA, respectively.

The components of the electrostatic quadrupole moment of each of the three squaraine molecules evaluated with both DMAs are equivalent within fractions of the pooled standard deviation. Therefore, we report in Table 9 only one of the two sets of calculated quantities, namely that coming from Stewart DMA. Both traceless cartesian tensors and spherical harmonic tensors are listed. For each molecule, the origin is at the centre of mass and the reference system is given by the eigen-axes of the inertial tensor.

Table 9. Molecular Electrostatic Multipole Moments in units of Debye·Å. Individual components are referred to the eigen-axes of the inertial tensor, with origin in the molecular centre of mass.

Moment	SQ	SQDH	
		Squaraine Sq1	**Squaraine Sq2**
Traceless Cartesian tensors			
$\langle xx \rangle$	32 ± 4	22 ± 5	35 ± 5
$\langle xy \rangle$	-4 ± 3	0.6 ± 3.7	-4 ± 4
$\langle yy \rangle$	-25 ± 2	-20 ± 3	-28 ± 3
$\langle xz \rangle$	4 ± 2	3 ± 2	2 ± 2
$\langle yz \rangle$	1.1 ± 0.7	-0.4 ± 1.0	1 ± 1
$\langle zz \rangle$	-7 ± 2	-2 ± 3	-7 ± 3
Anisotropy	7.1 ± 0.6	6.0 ± 0.6	7.5 ± 0.5
Spherical Harmonic Tensors			
$\langle 2, 2 \rangle$	33 ± 5	24 ± 4	36 ± 5
$\langle 2, -2 \rangle$	-5 ± 5	0.7 ± 4.3	-4 ± 4
$\langle 2, 1 \rangle$	4 ± 3	3 ± 2	3 ± 2
$\langle 2, -1 \rangle$	1 ± 1	-0.4 ± 1.2	2 ± 1
$\langle 2, 0 \rangle$	-7 ± 3	-2 ± 3	-7 ± 3

A quick look at the table shows the expected similarities among the three quadrupole tensors, with a few differences, which can be visualized in a graphical representation by means of a linear correlation between the values of pairs of quadrupole tensor components. The highest correlation coefficient R, 0.9987, is that between the SQ squaraine molecule and sq2, but the slope, equal to 1.108,

is a possible measure of the difference between the two electrostatic moments. Less satisfactory is the agreement between quadrupole moments of sq1 and sq2 or between sq1 and SQ molecules, because the corresponding correlation coefficients are 0.9875 for the first pair and 0.9829 for the second one, and the slopes are as large as 1.541 and 1.384, respectively. We believe that these values confirm the differences between the EDDs of the three molecules, a clue to limited transferability of electrostatic properties for the same molecule in different crystalline environments.

The values of the water dipole moment μ (in Debye units) from Stewart DMA are 1.68 ± 0.05 D for the most negative molecule (the one at O3) and 1.81 ± 0.05 D for the positive water molecule, while the calculation with the QTAIM DMA of the total electron density assigns larger μ values to both molecules, namely μ= 1.82 ± 0.04 D to the O3 water molecule and μ = 2.06 ± 0.03 D to the water molecule at O4. Literature values for this property in hydrated crystals [50,55], including both positively and negatively charged water molecules, are in the range of 1.59 to 2.44 D. In our case, the difference is largely due to the diverse values of the PAMoC integrated charges of the oxygen atoms, −0.98e for atom O3 and −0.92e for atom O4 (with esds < 0.01e).

Quadrupole moments of the two water molecules have also been obtained with both DMA methods. The Stewart DMA traceless tensors were calculated by PAMoC with the centre of mass as origin and the eigen-axes of the inertial tensor as reference system. The corresponding terms of the two tensors correlate with an R value of 0.9875, and the slope of the straight line is 1.046. The values of the two principal components, in units of 10^{-40} Cm^2, amount to +4.94 and −4.27 in the quadrupole tensor of the water molecule at O4 and to +4.37 and −4.37, respectively, in the tensor of the other H_2O molecule (at O3), where the third diagonal component is zero within fractions of the experimental error, estimated by PAMoC as equal to 0.07. Diffraction multipole results for these two quantities range from +3.3 to +11.0 and from −2.9 to −13.0 [50,55].

As with the dipolar moments, the quadrupoles obtained from the QTAIM DMA are also larger than those derived from the Stewart DMA. Furthermore, the values of the components of the quadrupole tensor of the water molecule at atom O4 are almost double those of the tensor of the other H_2O molecule. The components of the two tensors are correlated with an index R = 0.9796 and the straight line has a slope of 1.88 when the values of the tensor of H_2O at O3 are reported in the abscissas. The two largest diagonal terms of the two traceless tensors, expressed in the same units as above, are +5.87 and −6.00 for one molecule and +9.11 and −7.67 for the other. The reason for the discrepancy between the results from the two DMA is not evident. We suspect it might be related to a poor accuracy in the PAMoC integration of the H basins of the water molecules, a problem that does not affect the Stewart DMA calculation, which does not require any integration.

4. Conclusions

The three 1,3-bis(dimethylamino)squaraine molecules examined here in three distinct crystal environments have equivalent geometries but different electrostatic properties. The electron density topology of the two molecules in the dihydrate (SQDH) compound differs from that of the molecule in the anhydrous crystal (SQ). The presence of water molecules in SQDH modifies the charge density of the two squaraines, as is evident in the maps of the electrostatic potential of each molecule "extracted" from the crystal. There is no large difference in group volumes, but the group charges differ significantly. Quadrupolar tensors highlight similarities and differences.

A significant common aspect is the large positive charge of the squarylium ring. This refutes the theoretical results recently obtained for a bis(4-dimethylaminophenyl)squaraine, numbered 1 in [18], which differs from the one in our study for the insertion of phenyl rings between the four-carbon ring and the bisdimethylamino groups. Those theoretical calculations suggest the location of positive charge on NMe$_2$ groups. In the words of the authors of that study, "the typically used chemical structure drawing of 1 showing +2 charge on the squaraine ring is inaccurate and misleading." We believe that the presence of phenyl rings certainly modifies the electron density distribution, but hardly to the point of leaving a positive charge on the nitrogen atom, as inferred from the drawings in that paper.

Our PAMoC integration obtains values of −0.84 ± 0.01*e* for the N atom in the dihydrate crystal and −0.949 ± 0.008*e* in the anhydrous SQ. The positive charge of the squarylium ring exceeds +2*e* in all three molecules. Certainly, theoretical calculations on our squaraine at the same level of theory as that adopted for squaraine **1** [18], followed by topological analysis of the theoretical charge distributions of both, could help to clarify which is the more realistic description of the squarylium ring.

References

1.　Schmidt, A.H. Reaktionen von Quadratsäure und Quadratsäure-Derivaten. *Synthesis* **1980**, *1980*, 961–994. [CrossRef]

2.　Schmidt, A.H. The Chemistry of Squaraines. In *Oxocarbons*; Elsevier: Amsterdam, The Netherlands, 1980; pp. 185–231.

3.　Ajayaghosh, A. Chemistry of Squaraine-Derived Materials: Near-IR Dyes, Low Band Gap Systems, and Cation Sensors. *Acc. Chem. Res.* **2005**, *38*, 449–459. [CrossRef] [PubMed]

4.　Ilina, K.; MacCuaig, W.M.; Laramie, M.; Jeouty, J.N.; McNally, L.R.; Henary, M. Squaraine Dyes: Molecular Design for Different Applications and Remaining Challenges. *Bioconjugate Chem.* **2020**, *31*, 194–213. [CrossRef] [PubMed]

5.　Khopkar, S.; Shankarling, G. Synthesis, photophysical properties and applications of NIR absorbing unsymmetrical squaraines: A review. *Dye. Pigment.* **2019**, *170*, 107645. [CrossRef]

6.　Meier, H. Extended conjugation in stilbenoid squaraines. *Z. Nat. B* **2019**, *74*, 241–254. [CrossRef]

7.　Law, K.Y. Squaraine chemistry. A study of the solute-solvent complexation of squaraine in solvents by proton NMR spectroscopy. *J. Phys. Chem.* **1989**, *93*, 5925–5930. [CrossRef]

8.　SciFinder. Chemical Abstracts Service, Columbus (OH). Available online: https://scifinder.cas.org (accessed on 1 September 2020).

9.　Lunelli, B.; Roversi, P.; Ortoleva, E.; Destro, R. Geometry and molecular parameters of 3,4-bis(dimethylamino)-3-cyclobutene-1,2-dione and its isomer bis(dimethylamino)squaraine. Combined study by IR spectroscopy, XRD and ab initio MO calculations. *J. Chem. Soc. Faraday Trans.* **1996**, *92*, 3611. [CrossRef]

10.　Lunelli, B.; Roversi, P.; Ortoleva, E.; Destro, R. Corrigendum to Geometry and molecular parameters of 3,4-bis(dimethylamino)-3-cyclobutene-1,2-dione and its isomer bis(dimethylamino)squaraine: Combined study by IR spectroscopy, XRD and ab initio MO calculations. *J. Chem. Soc. Faraday Trans.* **1997**, *93*, 513.

11.　Lunelli, B.; Soave, R.; Destro, R. Structure and stability of bis(dimethylamino)squaraine and its hydrates: A study using XRD, IR spectroscopy, and thermodynamic measurements. *Phys. Chem. Chem. Phys.* **1999**, *1*, 1469–1477. [CrossRef]

12.　Chen, Z.; Lohr, A.; Saha-Möller, C.R.; Würthner, F. Self-assembled π-stacks of functional dyes in solution: structural and thermodynamic features. *Chem. Soc. Rev.* **2009**, *38*, 564–584. [CrossRef]

13.　Ashwell, G.J.; Jefferies, G.; Hamilton, D.G.; Lynch, D.E.; Roberts, M.P.S.; Bahra, G.S.; Brown, C.R. Strong second-harmonic generation from centrosymmetric dyes. *Nature* **1995**, *375*, 385–388. [CrossRef]

14.　Honeybourne, C.L. Charge distortion by sparkles can explain strong SHG by centrosymmetric squaraine dyes. *J. Mater. Chem.* **1999**, *9*, 2241–2244. [CrossRef]

15. Sissa, C.; Terenziani, F.; Painelli, A.; Siram, R.B.K.; Patil, S. Spectroscopic Characterization and Modeling of Quadrupolar Charge-Transfer Dyes with Bulky Substituents. *J. Phys. Chem. B* **2012**, *116*, 4959–4966. [CrossRef] [PubMed]

16. Sanyal, S.; Painelli, A.; Pati, S.K.; Terenziani, F.; Sissa, C. Aggregates of quadrupolar dyes for two-photon absorption: the role of intermolecular interactions. *Phys. Chem. Chem. Phys.* **2016**, *18*, 28198–28208. [CrossRef]

17. Orian, L.; Pilot, R.; Bozio, R. In Silico Stark Effect: Determination of Excited-State Polarizabilities of Squaraine Dyes. *J. Phys. Chem. A* **2017**, *121*, 1587–1596. [CrossRef]

18. Divya, V.V.; Suresh, C.H. Electronic Structure of Bis(4-dimethylaminophenyl)squaraine. *ChemistrySelect* **2019**, *4*, 3387–3394. [CrossRef]

19. Nazarov, A.E.; Ivanov, A.I.; Vauthey, E. Modeling Infrared Spectral Dynamics upon Symmetry Breaking of a Photo-Excited Quadrupolar Dye. *J. Phys. Chem. C* **2020**, *124*, 2357–2369. [CrossRef]

20. Destro, R. Detection and characterization of a reversible solid-solid phase transition at 147 K in crystalline 3,4-bis(dimethylamino)-3-cyclobutene-1,2-dione. *Chem. Phys. Lett.* **1997**, *275*, 463–468. [CrossRef]

21. Stewart, R.F.; Spackman, M.A. *VALRAY User's Manual*; Carnegie Mellon University: Pittsburgh, PA, USA; University of Copenhagen: Copenhagen, Denmark, 2000.

22. Samson, S.; Goldish, E.; Dick, C.J. A novel low-temperature X-ray goniometer with closed-cycle cooling to about 18 K. *J. Appl. Crystallogr.* **1980**, *13*, 425–432. [CrossRef]

23. Destro, R. Experimental Determination of Scan-truncation Losses from Low-temperature (16 K) Single-crystal X-ray Measurements. *Aust. J. Phys.* **1988**, *41*, 503. [CrossRef]

24. Destro, R.; Roversi, P.; Barzaghi, M.; Marsh, R.E. Experimental Charge Density of α-Glycine at 23 K. *J. Phys. Chem. A* **2000**, *104*, 1047–1054. [CrossRef]

25. Destro, R.; Marsh, R.E. Scan-truncation corrections in single-crystal diffractometry: an empirical method. *Acta Crystallogr. Sect. A Found. Crystallogr.* **1987**, *43*, 711–718. [CrossRef]

26. Destro, R.; Marsh, R.E. On predicting scan profiles: the nature of the 'aberration function'. *Acta Crystallogr. Sect. A Found. Crystallogr.* **1993**, *49*, 183–190. [CrossRef]

27. Stewart, R.F. Generalized X-Ray Scattering Factors. *J. Chem. Phys.* **1969**, *51*, 4569–4577. [CrossRef]

28. Stewart, R.F. Electron population analysis with rigid pseudoatoms. *Acta Crystallogr. Sect. A: Cryst. Physics, Diffr. Theor. Gen. Crystallogr.* **1976**, *32*, 565–574. [CrossRef]

29. NATO Advanced Study Institute. *The Application of Charge Density Research to Chemistry and Drug Design*; Jeffrey, G.A., Piniella, J.F., Eds.; Springer: Boston, MA, USA, 1991; Volume 250, ISBN 978-0-306-43880-6.

30. Roversi, P.; Destro, R. Approximate anisotropic displacement parameters for H atoms in molecular crystals. *Chem. Phys. Lett.* **2004**, *386*, 472–478. [CrossRef]

31. Barzaghi, M. PAMoC (version 2002.0) online User's Manual 2002. Available online: https://www.pamoc.it/ (accessed on 6 June 2020).

32. Steiner, T. C–H⋯O hydrogen bonding in crystals. *Crystallogr. Rev.* **2003**, *9*, 177–228. [CrossRef]

33. Koch, U.; Popelier, P.L.A. Characterization of C-H-O Hydrogen Bonds on the Basis of the Charge Density. *J. Phys. Chem.* **1995**, *99*, 9747–9754. [CrossRef]

34. Gatti, C.; May, E.; Destro, A.R.; Cargnoni, F. Fundamental Properties and Nature of CH⋅O Interactions in Crystals on the Basis of Experimental and Theoretical Charge Densities. The Case of 3,4-Bis(dimethylamino)-3-cyclobutene-1,2-dione (DMACB) Crystal. *J. Phys. Chem. A* **2002**, *106*, 2707–2720. [CrossRef]

35. Destro, R.; Sartirana, E.; Loconte, L.; Soave, R.; Colombo, P.; Destro, C.; Lo Presti, L. Competing C=O⋯C=O, C–H⋯O, Cl⋯O, and Cl⋯Cl Interactions Governing the Structural Phase Transition of 2,6-Dichloro-p-benzoquinone at Tc = 122.6 K. *Cryst. Growth Des.* **2013**, *13*, 4571–4582. [CrossRef]

36. Lo Presti, L.; Soave, R.; Destro, R. On the Interplay between CH⋯O and OH⋯O Interactions in Determining Crystal Packing and Molecular Conformation: An Experimental and Theoretical Charge Density Study of the Fungal Secondary Metabolite Austdiol (C12H12O5). *J. Phys. Chem. B* **2006**, *110*, 6405–6414. [CrossRef] [PubMed]

37. Bader, R.F.W. Atoms in Molecules: A Quantum Theory. In *International Series of Monographs on Chemistry 22*; Clarendon Press: Oxford, UK, 1990; ISBN 9780198558651.

38. Gajda, R.; Stachowicz, M.; Makal, A.; Sutuła, S.; Parafiniuk, J.; Fertey, P.; Woźniak, K. Experimental charge density of grossular under pressure—a feasibility study. *IUCrJ* **2020**, *7*, 383–392. [CrossRef] [PubMed]

39. Destro, R.; Ruffo, R.; Roversi, P.; Soave, R.; Loconte, L.; Lo Presti, L. Anharmonic motions versus dynamic disorder at the Mg ion from the charge densities in pyrope (Mg3Al2Si3O12) crystals at 30 K: Six of one, half a dozen of the other. *Acta Crystallogr. Sect. B Struct. Sci. Cryst. Eng. Mater.* **2017**, *73*, 722–736. [CrossRef] [PubMed]

40. Destro, R.; Ortoleva, E.; Soave, R.; Loconte, L.; Lo Presti, L. Detection and kinetics of the single-crystal to single-crystal complete transformation of a thiiranium ion into thietanium ion. *Phys. Chem. Chem. Phys.* **2009**, *11*, 7181. [CrossRef]

41. Lo Presti, L.; Ellern, A.; Destro, R.; Soave, R.; Lunelli, B. Rationalizing the Effect of Halogenation on the Molecular Structure of Simple Cyclobutene Derivatives by Topological Real-Space Analysis of Their Electron Density. *J. Phys. Chem. A* **2011**, *115*, 12695–12707. [CrossRef] [PubMed]

42. Lo Presti, L.; Orlando, A.M.; Loconte, L.; Destro, R.; Ortoleva, E.; Soave, R.; Gatti, C. Single N-C Bond Becomes Shorter than a Formally Double N=C Bond in a Thiazete-1,1-dioxide Crystal: An Experimental and Theoretical Study of Strong Crystal Field Effects. *Cryst. Growth Des.* **2014**, *14*, 4418–4429. [CrossRef]

43. Collard, K.; Hall, G.G. Orthogonal trajectories of the electron density. *Int. J. Quantum Chem.* **1977**, *12*, 623–637. [CrossRef]

44. Roversi, P.; Merati, F.; Destro, R.; Barzaghi, M. Charge density in crystalline citrinin from X-ray diffraction at 19 K. *Can. J. Chem.* **1996**, *74*, 1145–1161. [CrossRef]

45. Saleh, G.; Soave, R.; Lo Presti, L.; Destro, R. Progress in the Understanding of the Key Pharmacophoric Features of the Antimalarial Drug Dihydroartemisinin: An Experimental and Theoretical Charge Density Study. *Chem. A Eur. J.* **2013**, *19*, 3490–3503. [CrossRef]

46. Finocchio, G.; Rizzato, S.; Macetti, G.; Tusha, G.; Lo Presti, L. Unravelling the Chemistry of the [Cu(4,7-Dichloroquinoline)2Br2]2 Dimeric Complex through Structural Analysis: A Borderline Ligand Field Case. *Crystals* **2020**, *10*, 477. [CrossRef]

47. Budzelaar, P.H.M.; Dietrich, H.; Macheleid, J.; Weiss, R.; Schleyer, P.V.R. The molecular and electronic structure of dipiperidinosquaraine. *Eur. J. Inorg. Chem.* **1985**, *118*, 2118–2126. [CrossRef]

48. Bahtiar, A.; Tusaddiah, S.H.; Safriani, L. Improved charge carrier transfer in squaraine-capped ZnO nanoparticles layer for electron transport of hybrid solar cells. *J. Physics: Conf. Ser.* **2018**, *1080*, 012001. [CrossRef]

49. Hestand, N.J.; Zheng, C.; Penmetcha, A.R.; Cona, B.; Cody, J.A.; Spano, F.C.; Collison, C.J. Confirmation of the Origins of Panchromatic Spectra in Squaraine Thin Films Targeted for Organic Photovoltaic Devices. *J. Phys. Chem. C* **2015**, *119*, 18964–18974. [CrossRef]

50. Spackman, M.A. Molecular electric moments from x-ray diffraction data. *Chem. Rev.* **1992**, *92*, 1769–1797. [CrossRef]

51. Koritsanszky, T.S.; Coppens, P. Chemical applications of X-ray charge-density analysis. *Chem. Rev.* **2001**, *101*, 1583–1628. [CrossRef]

52. Bohorquez, H.J.; Obregon, M.; Cárdenas, C.; Llanos, E.; Suárez, C.; Villaveces, J.L.; Patarroyo, M.E. Electronic Energy and Multipolar Moments Characterize Amino Acid Side Chains into Chemically Related Groups. *J. Phys. Chem. A* **2003**, *107*, 10090–10097. [CrossRef]

53. Destro, R.; Soave, R.; Barzaghi, M. Physicochemical Properties of Zwitterionic L - and DL -Alanine Crystals from Their Experimental and Theoretical Charge Densities. *J. Phys. Chem. B* **2008**, *112*, 5163–5174. [CrossRef]

54. Cardamone, S.; Hughes, T.J.; Popelier, P.L.A. Multipolar electrostatics. *Phys. Chem. Chem. Phys.* **2014**, *16*, 10367. [CrossRef]

55. Coppens, P. *X-Ray Charge Densities and Chemical Bonding*; Oxford University Press: New York, NY, USA, 1997; ISBN 0-19-509823-4.